Signal transduction by BvgS sensor kinase

Elian Dupré, Elodie Lesne, Jérémy Guérin, Marc F. Lensink, Alexis Verger, Jerome de Ruyck, Guillaume Brysbaert, Herve Vezin, Camille Locht, Rudy Antoine, et al.

THE JOURNAL OF BIOLOGICAL CHEMISTRY VOL. 290, NO. 38, pp. 23307–23319, September 18, 2015

Signal Transduction by BvgS Sensor Kinase

*BINDING OF MODULATOR NICOTINATE AFFECTS THE CONFORMATION AND DYNAMICS OF THE ENTIRE PERIPLASMIC MOIETY**

Received for publication, March 30, 2015, and in revised form, July 9, 2015 Published, JBC Papers in Press, July 22, 2015, DOI 10.1074/jbc.M115.655720

Elian Dupré[‡§¶‖1,2], Elodie Lesne[‡§¶‖1], Jérémy Guérin[‡§¶‖], Marc F. Lensink[§], Alexis Verger[§**], Jérôme de Ruyck[§**], Guillaume Brysbaert[§**], Hervé Vezin[§‡‡], Camille Locht[‡§¶‖], Rudy Antoine[‡§¶‖3], and Françoise Jacob-Dubuisson[‡§¶‖4]**

*From the [‡]Institut Pasteur de Lille, Center for Infection and Immunity of Lille, 59019 Lille Cedex, France, the [§]Université Lille Nord de France, 59000 Lille, France, the [¶]CNRS, Unité mixte de recherche (UMR) 8204, 59046 Lille, France, the [‖]INSERM, U1019, 59045 Lille, France, the **Unité de Glycobiologie Structurale et Fonctionnelle, CNRS, UMR 8576, 59658 Villeneuve d'Ascq, France, and the [‡‡]Laboratoire de spectrochimie infrarouge et Raman (LASIR), CNRS, UMR 8516, 59658 Villeneuve d'Ascq, France*

Background: The sensor kinase BvgS controls *Bordetella* virulence and is modulated by nicotinate.
Results: Binding of nicotinate to the Venus flytrap domain affects the conformation and dynamics of the entire BvgS periplasmic moiety.
Conclusion: Mechanical transmission of signals perceived in the periplasm turn the cytoplasmic moiety to phosphatase.
Significance: Deciphering signal transmission in BvgS illuminates regulation by sensor kinases with Venus flytrap perception domains.

The two-component sensory transduction system BvgAS controls the virulence regulon of the whooping-cough agent *Bordetella pertussis*. The periplasmic moiety of the homodimeric sensor kinase BvgS is composed of four bilobed Venus flytrap (VFT) perception domains followed by α helices that extend into the cytoplasmic membrane. In the virulent phase, the default state of *B. pertussis*, the cytoplasmic enzymatic moiety of BvgS acts as kinase by autophosphorylating and transferring the phosphoryl group to the response regulator BvgA. Under laboratory conditions, BvgS shifts to phosphatase activity in response to modulators, notably nicotinate ions. Here we characterized the effects of nicotinate and related modulators on the BvgS periplasmic moiety by using site-directed mutagenesis and *in silico* and biophysical approaches. Modulators bind with low affinity to BvgS in the VFT2 cavity. Electron paramagnetic resonance shows that their binding globally affects the conformation and dynamics of the periplasmic moiety. Specific amino acid substitutions designed to slacken interactions within and between the VFT lobes prevent BvgS from responding to nicotinate, showing that BvgS shifts from kinase to phosphatase activity in response to this modulator via a tense transition state that involves a large periplasmic structural block. We propose that this transition enables the transmembrane helices to adopt a distinct conformation that sets the cytoplasmic enzymatic moiety in the phosphatase mode. The *bona fide*, *in vivo* VFT ligands that remain to be identified are likely to trigger similar effects on the transmembrane and cytoplasmic moieties. This mechanism may be relevant to the other VFT-containing sensor kinases homologous to BvgS.

Two-component systems represent major signal transduction pathways in bacteria (1). They regulate important cellular programs that enable bacteria to adapt to physical or chemical changes in their environment. Prototypical two-component systems are composed of a sensor kinase and a response regulator, serving as a signal receptor and effector, respectively (2, 3). Each component protein harbors distinct functional domains (4). Signal perception by the extracytoplasmic domain of the sensor kinase triggers autophosphorylation of a conserved His of the cytoplasmic dimerization and His phosphostransfer (DHp) domain. Phosphotransfer then occurs between the phosphohistidine and a conserved Asp residue in the receiver domain of the response regulator (4). Many response regulators act as transcriptional activators when phosphorylated.

The BvgAS two-component system of the whooping cough agent *Bordetella pertussis* controls the expression of the virulence regulon (5, 6). The sensor kinase BvgS phosphorylates the transcriptional activator BvgA at 37 °C under standard laboratory conditions and media, setting the bacteria in the Bvg^+ phase in which the virulence regulon is transcribed. The Bvg^+ phase appears to be the default phase of *B. pertussis*. Conversely, low temperatures or millimolar concentrations of chemical modulators such as nicotinate or sulfate ions turn off the kinase activity of BvgS and turn on its phosphatase activity. The virulence genes are no longer transcribed, and a small set of virulence-repressed genes is up-regulated. This sets the bacte-

* This work was supported by Grant ANR-13-BSV8 – 0002-01 from the Agence Nationale de la Recherche (to F. J. D.). This research used resources from the Plateforme Technologique de Calcul Intensif at the University of Namur, Belgium, which is supported by the Fonds de la Recherche Scientifique (F. R. S.)-FNRS under convention 2.4520.11. The authors declare that they have no conflict of interest with the contents of this manuscript.
[1] Both authors contributed equally to this work.
[2] Recipient of predoctoral fellowships from the French Research Ministry and the Fonds de la Recherche Médicale.
[3] To whom correspondence may be addressed: Center for Infection and Immunity of Lille, Institut Pasteur de Lille, 1 rue Calmette, 59019 Lille Cedex, France. Tel.: 33-320-87-11-51; Fax: 33-320-87-11-58; E-mail: rudy.antoine@pasteur-lille.fr.
[4] To whom correspondence may be addressed: Center for Infection and Immunity of Lille, Institut Pasteur de Lille, 1 rue Calmette, 59019 Lille Cedex, France. Tel.: 33-320-87-11-55; Fax: 33-320-87-11-58; E-mail: francoise.jacob@ibl.cnrs.fr.

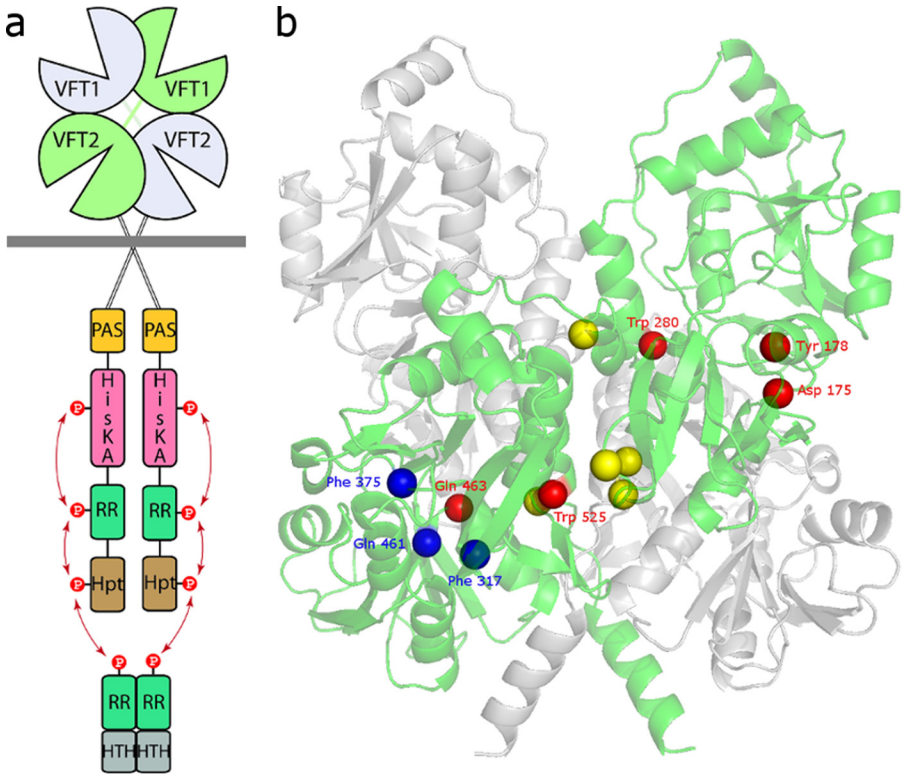

FIGURE 1. **The sensor-kinase BvgS**. *a*, schematic of the BvgS dimer. From the N to the C terminus, each monomer is composed of two periplasmic VFT domains, a transmembrane segment, and a PAS domain, followed by histidine kinase (*HisKA*), receiver (*RR*), and histidine phosphotransfer domains that make up a phosphorelay (*arrows*). BvgA is composed of a receiver domain and a DNA-binding (helix turn helix, *HTH*) domain and also forms dimers. *b*, schematic of the periplasmic moiety of BvgS. One monomer is colored *green* and the second one *gray*. The positions of the substitutions described in this work that prevent modulation by nicotinic acid are shown as *red spheres* centered on the Cα of each residue. The positions of previously described substitutions that similarly cause an unresponsive phenotype (21) are shown as *yellow spheres* (D160A, F230A, N231A, S287A, and R526A). Positions of the substitutions in the VFT2 cavity that are used in this work are shown as *blue spheres*. The substitutions are shown only for the green monomer.

ria in the avirulent, Bvg^- phase. An intermediate phase occurs at moderate modulator concentrations, in which only the "early" virulence genes are transcribed together with intermediate genes (5, 7–9). The different phases of *B. pertussis* might correspond to distinct stages in the development of the infectious cycle. The natural, *in vivo* signals perceived by BvgS in its host remain to be identified.

Structure/activity relationship studies of nicotinate analogs have revealed that a planar aromatic ring structure and a carboxylate group are necessary for modulation (10, 11). Therefore, isonicotinate and chloronicotinate are modulators whereas nicotinamide is not. With its electron-withdrawing substituent, chloronicotinate modulates BvgS at lower concentrations than nicotinate. Non-aromatic carboxylic acids such as acetate or succinate do not modulate BvgS activity (10, 11).

Nicotinate and related modulators act on the periplasmic portion of BvgS (12–14), which is composed of extracytoplasmic Venus flytrap (VFT)[5] domains in tandem (Fig. 1) (15). VFT domains consist of two lobes delimitating a cavity and joined by a hinge. Those domains have been widely adopted throughout the phylogenetic tree for transport or signal perception purposes (16–18). Typically, ligand binding in the interlobe cavity of a VFT domain leads to clamshell motions that enclose the ligand (16, 19). In the case of signaling, this conformational change triggers downstream cellular events (17, 20). BvgS is the prototype of a large family of bacterial sensor kinases harboring tandem VFT domains whose mechanisms of signal perception and transduction remain to be deciphered (21).

The periplasmic portion of BvgS forms an intricate homodimer with open, membrane-distal VFT1 domains and closed, membrane-proximal VFT2 domains (21) (Fig. 1). They are followed by one helix per protomer, H19, which extends into the membrane to form a transmembrane region leading to a cytoplasmic Per/Arnt/Sim (PAS) domain and then to kinase, receiver, and histidine phosphotransfer domains involved in a phosphorelay (Fig. 1). The conformation of the periplasmic moiety determines the mode of activity of BvgS. In the Bvg^+ phase, the periplasmic portion of BvgS exerts a strain on the transmembrane helices that sets the cytoplasmic enzymatic moiety in a mode of high kinase and phosphotransferase activity (referred to below as the kinase mode) (21). How signal perception translates into a shift to a low-kinase, high-phosphatase mode of activity (hereafter called the phosphatase mode) remains to be determined. In this work, we characterized the effects of signal perception on BvgS and identified the features of the periplasmic domain necessary for the transition from the kinase to the phosphatase mode of activity by combining mutagenesis and biophysical methods. For want of the authentic BvgS ligand(s), we used nicotinate with the rationale that the

[5] The abbreviations used are: VFT, Venus flytrap; PAS, Per/Arnt/Sim; CWEPR, continuous wave electron paramagnetic spectroscopy; ITC, isothermal titration calorimetry.

mechanisms thus revealed would illuminate how the natural signals perceived by the periplasmic domains of BvgS regulate its enzymatic activity.

Experimental Procedures

Plasmids and Strains—Recombinant *B. pertussis* BPSM derivatives containing chimeric *bvgS* genes were constructed by allelic exchange as in Ref. 13. *lacZ* in transcriptional fusion with the sequence of the first gene of the pertussis toxin operon (22) was introduced into the different strains to measure BvgS kinase activity.

To enhance the formation of the dimeric form of the BvgS VFT domains, a recombinant protein with a C-terminal leucine zipper domain was constructed by overlapping PCR. The sequence for the zipper was amplified from pT18-zip (23) using the 5′-caacgtatgaaacagctggaaga-3′ and 5′-tactcgagcccacgttcaccaccagttt-3′ oligonucleotides as primers, and the 3′ part of the VFT2 sequence was amplified using the 5′-acagcatttcgaacgacgagc-3′ and 5′-tcttccagctgtttcatacgttgctcgttgcggtaggcgtacca-3′ primers. The amplicon resulting from the overlapping PCR was used to replace the XhoI-SfuI fragment of pGEV-VFT1+VFT2 (21). The resulting pGEV-BvgSpZIP plasmid codes for the two VFT domains preceded by a 60-residue GB1 carrier domain (24) and followed by two Gly residues and a Leu zipper. The E113C and N177C substitutions were introduced by overlapping PCR, and the resulting amplicons were restricted with BamHI and SfuI and introduced into pGEV-BvgSpZIP by ligation to replace the WT fragment. The L316C and D442C substitutions were introduced in pGEV-BvgSpZIP by site-directed mutagenesis on a pUC19 derivative containing the relevant *bvgS* fragment. Fragment exchange in pGEV-BvgSpZIP was performed as above.

The plasmids encoding the BvgS-p variants were obtained by the exchange of restriction fragments. A DraIII-SfuI fragment from pUC19mosaic containing the F317A substitution (14) was coligated with the BamHI-DraIII fragment from pGEV-VFT1+VFT2 in pGEV-BvgSpZIP restricted with BamHI-SfuI. MfeI and BstBI were used to combine the F375E/Q461E or Q463A substitution with the N177C or L316C substitution in pGEV-BvgSpZIP. SexAI and MfeI were used to combine the W525A substitution with the N177C or L316C substitution, and DraIII and MfeI were used to construct the plasmids with the W175A/Y178A substitutions and the E113C or L316C substitutions.

To prepare anti-BvgA antibodies, *bvgA* was amplified by PCR using the 5′-ggatcctacaacaaagtcctcatcattgac-3′ and BvgA-Lo 5′-aagcttctaggcgagattgttgcgtttg-3′ primers, and the amplicon was introduced into pQE30 (Qiagen). A second PCR was then performed to amplify *bvgA* with the sequence of the His_6 tag using 5′-ccatggcgcatcaccatcaccatcacg-3′ and BvgA-Lo. The amplicon was introduced into pET24d (Novagen), yielding pT7-H-BvgA, which was used to transform BL21(DE3) for protein production.

Isothermal Titration Calorimetry—Recombinant BvgS-p_{WT} and BvgS-p_{F317A} were produced and purified as described previously (21) and concentrated to 100 μM (6.9 mg/ml) before overnight dialysis against 100 mM HEPES (pH 8), 150 mM NaCl, and 150 mM imidazole. The dialysis buffer was used to prepare a 2 mM solution of nicotinate or chloronicotinate. The thermodynamic parameters were determined using an iTC200 calorimeter (MicroCal Malvern) at 25 °C. Preliminary data showed weak binding affinities and had c values lower than 1.0 stemming from the low availability of protein. However, a reliable binding constant can be obtained at low c values using high ligand concentrations (25). For binding of chloronicotinate to BvgS-p_{F317A}, a 2 mM solution was titrated into the sample cell containing 25 μM of BvgS-p_{F317A}. The ligand concentration was about 80 times that of the protein so that the final molar ratio of ligand:protein at the end of the titration was 15:20. Injection steps were 2 μl (first injection, 0.4 μl) with 120-s spacing. Baseline corrections were performed by titrating ligand into sample buffer. Data were processed using Origin 7 software (OriginLab) and fitted using a single binding site mechanism where n was fixed at 2.

Microscale Thermophoresis—Recombinant BvgS-p_{WT} and BvgS-p_{F317A} concentrated to 40 μM (2.8 mg/ml) were dialyzed overnight against 50 mM HEPES (pH 7.5), 150 mM NaCl, and 0.05% Tween 20. The dialysis buffer was used to prepare 100 mM solutions of nicotinate, chloronicotinate, and nicotinamide, and the pH was adjusted to 7.5 with NaOH. Proteins were fluorescently labeled using the Monolith NT protein labeling kit RED-NHS (NanoTemper Technologies) after dilution to 10 μM in the labeling buffer and using a dye:protein molar ratio of 3:1. The labeled proteins were diluted to 20 nM and mixed with equal volumes of a 1:1 serial dilution of the unlabeled ligands, yielding a concentration range from 50 mM to 1.5 μM. After 5 min of incubation, samples were loaded into standard capillaries (NanoTemper Technologies), and thermophoresis was measured using a Monolith NT.115 instrument (NanoTemper Technologies) at 25 °C with 5 s/30 s/5 s laser off/on/off times. Instrument parameters were adjusted with 40% light-emitting diode power and 20% IR laser power. Data from three independently pipetted measurements were analyzed using the signal from thermophoresis + T-jump for nicotinate and thermophoresis for chloronicotinate.

β-Galactosidase Measurements—Experiments were carried out as in Ref. 26. Briefly, *B. pertussis* was grown on Bordet-Gengou agar plates for 2 days at 37 °C and then cultured in modified Stainer Scholte medium for 24 h at 37 °C. This culture was used to inoculate Stainer Scholte medium containing the indicated modulator concentrations at an A_{600} of 0.1. The bacteria were grown to an A_{600} of 1.5, and they were harvested by centrifugation. They were lysed using a Hybaid Ribolyser apparatus (30 s at speed 6 in tubes containing 0.1-mm silica spheres as the lysing matrix). β-galactosidase activity was determined as in Ref. 22.

Phos-Tag Assay—B. pertussis BPSM was cultured as above. For kinetics experiments, the starting point (time 0) at which nicotinate or an analog was added corresponds to an A_{600} of 1.5. Cells from 2 ml of culture were then harvested at the indicated time points. Lysis was carried out in 100 mM sodium phosphate (pH 7), 10 mM KCl, and 1 mM $MgSO_4$ using the Ribolyser apparatus. The lysates were cleared by centrifugation for 15 min at 10,000 × *g*. Samples were mixed with loading solution at a 1:4 ratio (final composition of 1% SDS, 65 mM Tris-Cl (pH 8), 25% glycerol, and 0.5% bromphenol blue) before loading 3 μl onto a

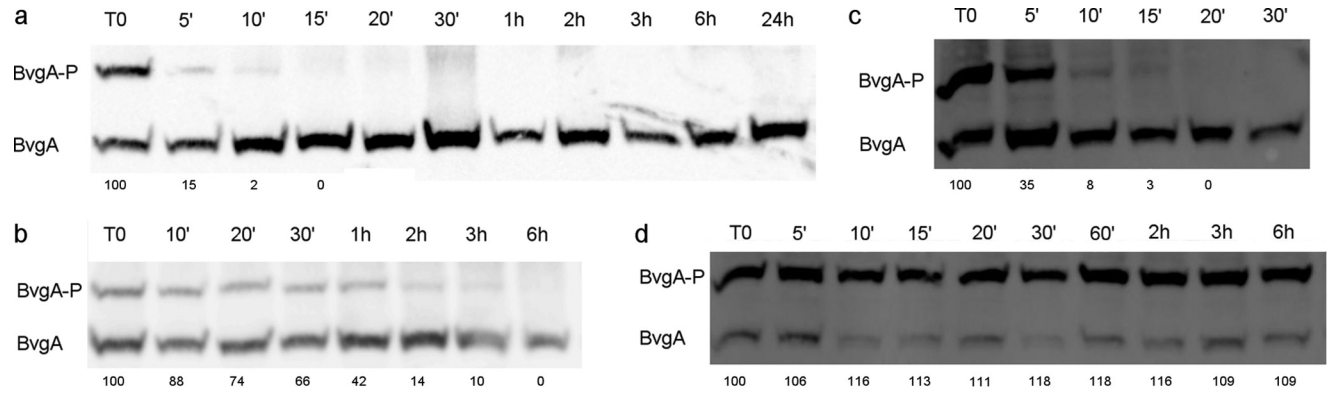

FIGURE 2. **Nicotinate triggers fast dephosphorylation of BvgA *in vivo*.** *a*, 8 mM nicotinic acid was added to *B. pertussis* cultures at time 0 (*T0*). Aliquots taken at the indicated times (in minutes and hours) were analyzed by electrophoresis in Phos-tag gels and immunoblotting using antibodies raised against BvgA. *b*, spontaneous dephosphorylation of BvgA. A lysate of *B. pertussis* grown under Bvg^+ conditions was incubated for the indicated times at 37 °C. Aliquots were subjected to Phos-tag analysis as in *a*. *c* and *d*, the dephosphorylation of BvgA was performed as in *a* after the addition of chloronicotinate to 1 mM (*c*) or of the non-modulating analog nicotinamide to 10 mM (*d*). The numbers below the panels show the proportions of phosphorylated BvgA present in each lane relative to the amount present at time 0.

SuperSep Phos-tag 12.5% gel (Wako Chemicals). Electrophoresis was performed at a constant voltage of 150 V at 4 °C for 1 h 15 min in 0.1 M Tris-Cl, 0.1 M MOPS (pH 8), 0.1% SDS, and 5 mM sodium bisulfite. Gels were then washed once in transfer buffer (25 mM Tris base, 0.192 M glycine, and 10% methanol) containing 1 mM EDTA for 10 min at room temperature and then twice for 15 min with transfer buffer. Following the electrotransfer, the immunoblots were saturated with milk and then incubated using polyclonal antibodies raised in guinea pigs against recombinant BvgA purified on a Ni^{2+} column in the presence of urea (Eurogentec). The antibodies were diluted 1:1000. The secondary antibodies (anti-guinea pig IgG HRP-conjugated, Jackson ImmunoResearch Laboratories) were diluted 1:10,000. The blots were developed using the Amersham Biosciences ECL Prime Western blotting detection system (GE Healthcare) and analyzed using a Fuji LAS-3000 imaging system. Quantification of the bands was performed using ImageQuantTL software (GE Healthcare).

Continuous Wave Electron Paramagnetic Spectroscopy (CWEPR)—The BvgS-p variants were produced and purified as in Ref. 21, except that 0.5 mM tris(2-carboxyethyl)phosphine (Sigma) was added to the clarified lysates before metal chelate chromatography. 0.5 mM EDTA was added to the purified proteins to remove traces of nickel. The proteins were mixed with a 10-fold molar excess of ((1-oxyl-2,2,5,5-tetramethyl-Δ3-pyrroline-3-methyl)methanethiosulfonate) (MTSL) (Toronto Research Chemicals) and incubated under gentle overnight agitation at 4 °C. A gel filtration step was performed using a PD10 column (GE Healthcare) pre-equilibrated with 10 mM Tris-HCl (pH 8.8) and 150 mM NaCl. The elution fractions were concentrated on an Amicon Ultra 4-10K column (Millipore) (10 min, 4000 × *g*, 16 °C).

Spin-labeled BvgS-p (80–100 μM) was injected into a glass capillary tube. CWEPR spectra were recorded at 296 K on an ESP 300E Bruker spectrometer equipped with an ELEXSYS super high sensitivity resonator operating at 9.8 GHz, and the microwave power was set to 10 milliwatt with a magnetic field modulation frequency of 100 kHz and an amplitude of 0.1 milliTesla. The samples were recorded with an accumulation of 6 or 10 spectra depending on labeling efficiency. For the modulated spectra, the indicated modulators were mixed with the protein before the measurements. The spectra were normalized for presentation. The simulations of the CWEPR spectra were performed with the Easyspin software package (Chili) under Matlab (27).

In Silico Modeling—Simulation of the complexes between nicotinate and VFT2 (PDB code 3MPK) was carried out using GOLD (version 5.0), which is based on a genetic algorithm (28). Docking simulations were performed on flexible ligands into protein structures with partial flexibility in the neighborhood of the active site. The torsion angles of Ser, Thr, and Tyr hydroxyl groups as well as Lys NH_3^+ moieties were optimized during the run so that hydrogen bond formation is favored. Default settings for genetic algorithm parameters and the ChemPLP scoring function were used. The interaction sphere was centered on the VFT2 hinge, represented by the Cα atom of Ala^{489} and delimited by a 20-Å radius. Water molecules were removed. Visual examination of the docking solutions was carried out with PyMOL (PyMOL molecular graphics system, version 1.5.0.4 Schrödinger, LLC). Molecular dynamics simulations were prepared and performed using the Gromacs suite of programs (29) using a dodecahedron system box with a minimum distance of 0.6 nm between the protein and box edges. Electrostatic neutrality was ensured by adding the appropriate amount of Na^+ counterions, and the system was equilibrated with 1000 steepest descent energy minimization followed by a short (20-ps) molecular dynamics run with frozen protein coordinates. The production run of 200 ns used settings as described in Ref. 21. Force field parameters for nicotinate will be described elsewhere.

Results

Shift of BvgS Activity upon Nicotinate Addition—To directly follow the enzymatic activity of BvgS after nicotinate addition, we used a Phos-tag assay that detects the kinase and phosphotransferase activities of BvgS via the level of phosphorylated BvgA (BvgA∼P) (30). Nicotinate was added to the bacterial cultures, and aliquots were taken after increasing periods of time. Detectable BvgA∼P disappears minutes after modulation (Fig. 2*a*). In contrast, compared with the fast dephosphoryla-

tion observed in the presence of nicotinate, the spontaneous dephosphorylation of BvgA in crude bacterial extracts incubated at 37 °C in the absence of a modulator is slow, indicating that the phosphorylated form of the response regulator is stable (Fig. 2*b*).

To confirm that the effect of nicotinate is specific, we also treated the bacteria with nicotinamide, a non-modulated molecule, and with chloronicotinate, which modulates BvgS activity *in vivo* at lower concentrations than nicotinate (11). Similar to nicotinate, the addition of millimolar concentrations of chloronicotinate, but not nicotinamide, causes a rapid shift of enzymatic activity of BvgS from a kinase to a phosphatase of BvgA, arguing that the *in vivo* effect of modulators is fast and specific (Fig. 2, *c* and *d*). Nicotinate and related modulating molecules can therefore be used as model signals to decipher the molecular mechanisms by which BvgS activity is regulated.

Binding of Nicotinate to BvgS—To characterize the interaction of modulators with the recombinant periplasmic dimer (BvgS-p), we performed isothermal titration calorimetry (ITC) experiments. However, no interpretable binding curve was obtained, indicating that the affinity may be too low for ITC and consistent with the millimolar concentrations necessary for *in vivo* effects. We therefore tested BvgS-p_{F317A} because the F317A substitution increases the sensitivity of BvgS to modulation (14), and we used chloronicotinate because it modulates BvgS at low concentrations (10, 11). Using BvgS-p_{F317A} with chloronicotinate, we could fit the ITC data with two equivalent binding sites per dimer and a K_d of around 200 μM (Fig. 3*a*).

MicroScale thermophoresis (31, 32) was used to confirm the ITC data. This technique allows for the analysis of protein-ligand interaction from nanomolar to micromolar affinity in solution by monitoring changes in protein diffusion between bound and unbound states across a laser-induced temperature gradient. We therefore determined the binding affinities of BvgS-p_{F317A} for chloronicotinate and nicotinate, with K_d values of close to 200 and 1200 μM, respectively (Fig. 3*b*). No binding was observed when nicotinamide was used as a control. WT BvgS-p showed bound and unbound states using chloronicotinate and nicotinate, but no K_d could be determined.

The ITC and thermophoresis data therefore indicate that BvgS harbors a low-affinity binding site per monomer for those modulators, although we cannot exclude the possibility of additional sites. The K_d values measured with the two methods are in line with the *in vivo* modulating concentrations (14).

The effect of Nicotinate Depends on the VFT2 Conformation—We have shown previously that nicotinate and related modulators raise the denaturation temperature of the recombinant VFT2 protein (14). Two sets of VFT2 cavity substitutions have opposite effects. The F317A substitution increases both the *in vivo* sensitivity of BvgS to modulation and the thermal stabilization of VFT2 by nicotinate, whereas, conversely, the F375E/Q461E substitutions that alter the positive electrostatic potential of the cavity abolish both the in *vivo* and *in vitro* effects of nicotinate (14). Collectively, these observations indicate that nicotinate exerts its effect on BvgS by binding to VFT2.

To investigate the effect of the modulator on the periplasmic moiety of BvgS for signaling, we introduced two distinct disulfide (S-S) bonds, Cys^{355}–Cys^{442} and Cys^{316}–Cys^{445}, across the

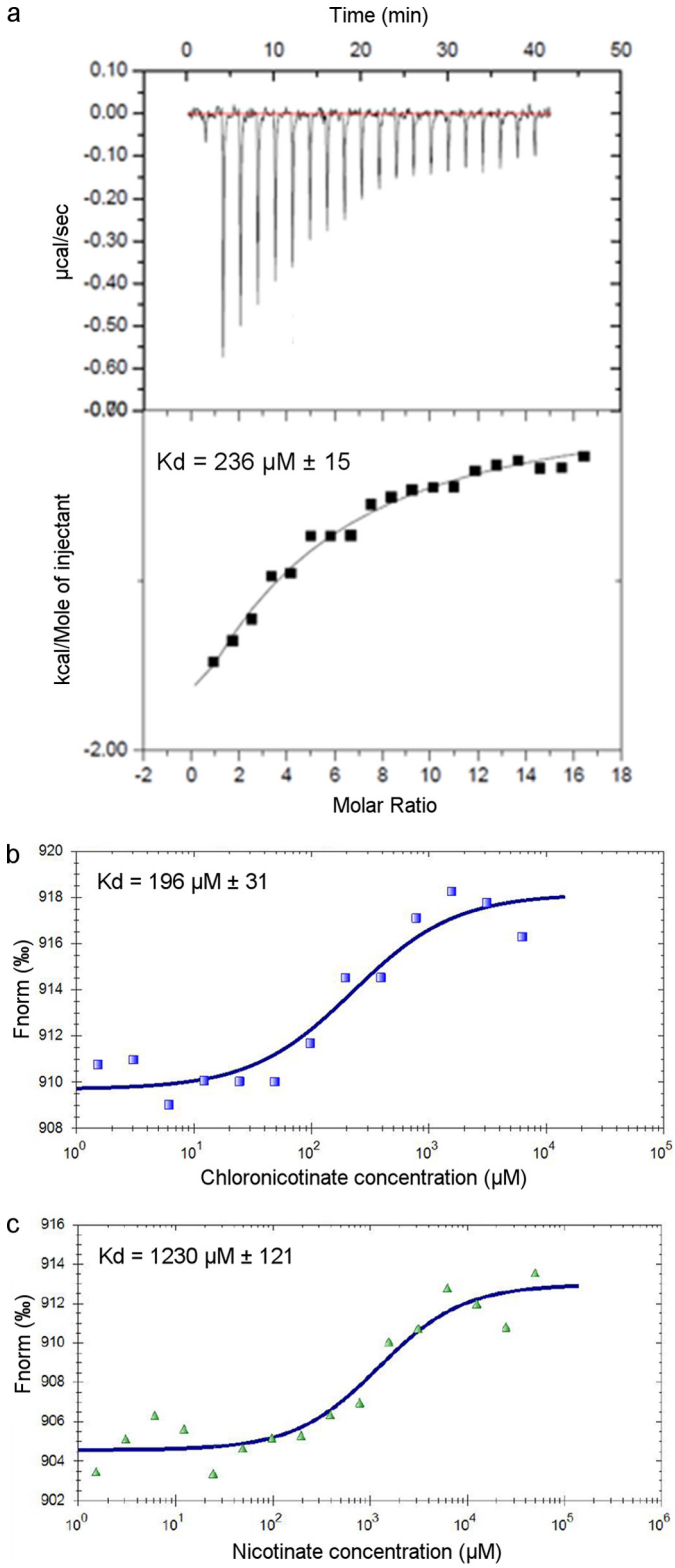

FIGURE 3. **Characterization of *in vitro* binding of modulators to BvgS.** *a*, chloronicotinate binding to BvgS-p_{F317A} using isothermal titration calorimetry. The ITC trace and the binding curve that fit the data using a single binding site per monomer model are shown. *b* and *c*, binding curves of chloronicotinate and nicotinate, respectively, to BvgS-p_{F317A} as determined by thermophoresis. A representative curve is shown in both cases, and the K_d values were calculated from three separate measurements for each modulator.

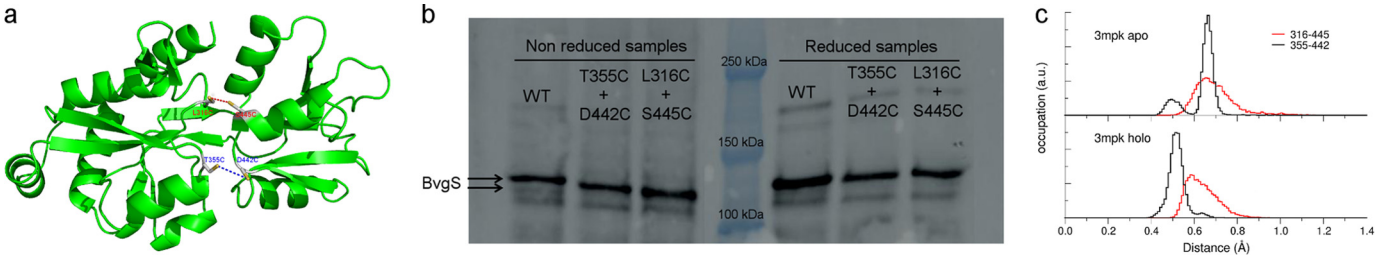

FIGURE 4. **Two distinct disulfide bonds across the VFT2 cavity have opposite effects on the response to nicotinate.** *a*, two S-S bonds were introduced across the interlobe cavity. The Cys^{316}–Cys^{445} S-S bond (*red*) increases BvgS sensitivity to nicotinate, whereas the Cys^{355}–Cys^{442} bond (*blue*) has the opposite effect (see Fig. 5). *b*, immunoblot analyses showing the BvgS variants in membrane extracts of *B. pertussis*. The samples were not reduced prior to electrophoresis, and, therefore, the S-S bond variants migrate slightly faster than WT BvgS (*left*). β-mercaptoethanol was added to the samples (*right*). *c*, distributions of the distances between Leu^{316} and Ser^{445} and between Thr^{355} and Asp^{442} over the course of molecular dynamics simulations of VFT2 (PDB code 3MPK), alone (*top*, *apo*) or with nicotinate in the interlobe cavity (*bottom*, *holo*). Histograms represent the fractional occupancy of the distances between the α carbons of Leu^{316} and Ser^{445} (*red*) and of Thr^{355} and Asp^{442} (*black*).

VFT2 cavity between the two lobes (Fig. 4*a*). The rationale was that with a S-S bond-locked VFT2, BvgS might fail to bind to, and to respond to, nicotinate. The BvgS variants were expressed in *B. pertussis* (Fig. 4*b*), and we assessed the response of BvgS to nicotinate using a reporter system in which the Bvg-regulated *ptx* promoter controls the expression of *lacZ* (13). Like the WT protein, both $BvgS_{C355\text{-}C442}$ and $BvgS_{C316\text{-}C445}$ are in the kinase mode under standard culture conditions, but, remarkably, they cause opposite nicotinate sensitivity phenotypes. Therefore, $BvgS_{C355\text{-}C442}$ is not modulated by nicotinate, whereas, in contrast, $BvgS_{C316\text{-}C445}$ is more sensitive than WT BvgS (Fig. 5). The addition of a reducing agent to the bacteria restores WT modulation phenotypes in both cases (Fig. 5). That these S-S bonds differently affect the *in vivo* response of BvgS to nicotinate suggests that the transition to the phosphatase mode triggered by the modulator involves a conformational change of the VFT2s that is facilitated by the Cys^{316}–Cys^{445} bond but hampered by the Cys^{355}–Cys^{442} bond.

We analyzed this further by performing molecular dynamics simulations of the VFT2 structure and measuring the evolution over time of the distances between the Cα atoms of the pairs of residues involved in the S-S bonds described above. For the 355–442 pair, two distance distributions are observed at roughly 5 and 6.6 Å, with a preference for the latter (Fig. 4*c*). For the 316–445 pair, a much broader distance distribution is observed, with a peak at 6.7 Å.

Using the VFT2 structure (PDB code 3MPK), we performed *in silico* molecular mechanics docking to identify a binding site. Analysis of the top-ranking solutions revealed a loose binding pocket in the cavity surrounded by hydrophobic and polar residues. When the docking assays were performed with the $BvgS_{F375E/Q461E}$ variant that is insensitive to nicotinate (14), no binding pocket was found. Molecular dynamics simulations were then performed with nicotinate in the VFT2 cavity, starting from the position defined with the docking procedure. Both sets of distances decrease, which suggests that nicotinate stabilizes a more compact form of VFT2 (Fig. 4*c*). That the two S-S bonds differently affect the *in vivo* response to nicotinate suggests that the Cys^{316}–Cys^{445} S-S bond facilitates the stabilization of the compact form by keeping the 316–445 distance short, resulting in a hypersensitive form of BvgS. In contrast, the Cys^{355}–Cys^{442} bond most likely opposes the conformational change of VFT2, resulting in an unresponsive phenotype. The data therefore support the idea that nicotinate binding makes the lobes of VFT2 move relative to one another. The resulting distortion of the VFT2 domains mechanically triggers a shift of enzymatic activity of the cytoplasmic domain.

The Integrity of the VFT Domains Determines the Response to Modulation—The lobes of VFT domains are considered rigid bodies. To address the importance of lobe integrity for modulation, we replaced specific residues whose side chains are involved in interactions that contribute to maintaining the lobe structure with Ala. We then determined the response of the BvgS variants to nicotinate using *ptx-lacZ* transcriptional fusion. The first lobes of the VFT1 domains (hereafter called $VFT1_{L1s}$) are connected to their respective H8 helices at the center of the dimer by a Trp residue conserved in the BvgS family, Trp^{280} (Fig. 1). The W280A substitution makes BvgS highly sensitive to nicotinate (Fig. 5). In the second lobes of VFT1s ($VFT1_{L2s}$) we simultaneously replaced Asp^{175} and Tyr^{178} with Ala. Asp^{175} connects the $VFT1_{L2}$ β sheet to α helix H5 in the same lobe, and Tyr^{178} points to the VFT1 hinge. The $BvgS_{D175A/Y178A}$ variant is unresponsive to nicotinate (Fig. 5).

In VFT2, Trp^{525} located in the α helix H18 is in a similar position as Trp^{280} in VFT1 and connects each $VFT2_{L1}$ to H18 at the center of the dimer (Fig. 1). In contrast with the W280A substitution, W525A makes BvgS insensitive to nicotinate (Fig. 5). Similarly, the Q463A substitution in $VFT2_{L2}$ abolishes the response to nicotinate (Fig. 5). The side chain of Gln^{463} makes both intra-VFT2 and inter-$VFT2_{L2}$-$VFT1_{L2}$ H-bonds (21).

Therefore, the two lobes of VFT1 appear to differently affect the transition to the phosphatase mode induced by nicotinate. The integrity of the second lobe is necessary for the transition, whereas, in contrast, a looser first lobe facilitates the response to the modulator. In VFT2, slackening either lobe hampers the shift of BvgS to the phosphatase mode. The integrity of $VFT1_{L2s}$, $VFT2_{L1s}$, and $VFT2_{L2s}$ is therefore necessary for the transition. In line with this, we have shown previously that tight inter-VFT1-VFT2 interactions are also necessary for the response to nicotinate (21).

To probe the interplay between VFT domains, we combined specific substitutions and determined the *in vivo* response to nicotinate using the *ptx-lacZ* reporter. The F375E/Q461E substitutions in the VFT2 cavity, which cause an unresponsive phenotype, were combined with W280A in $VFT1_{L1}$, which gives a hypersensitive phenotype. The resulting BvgS variant is insen-

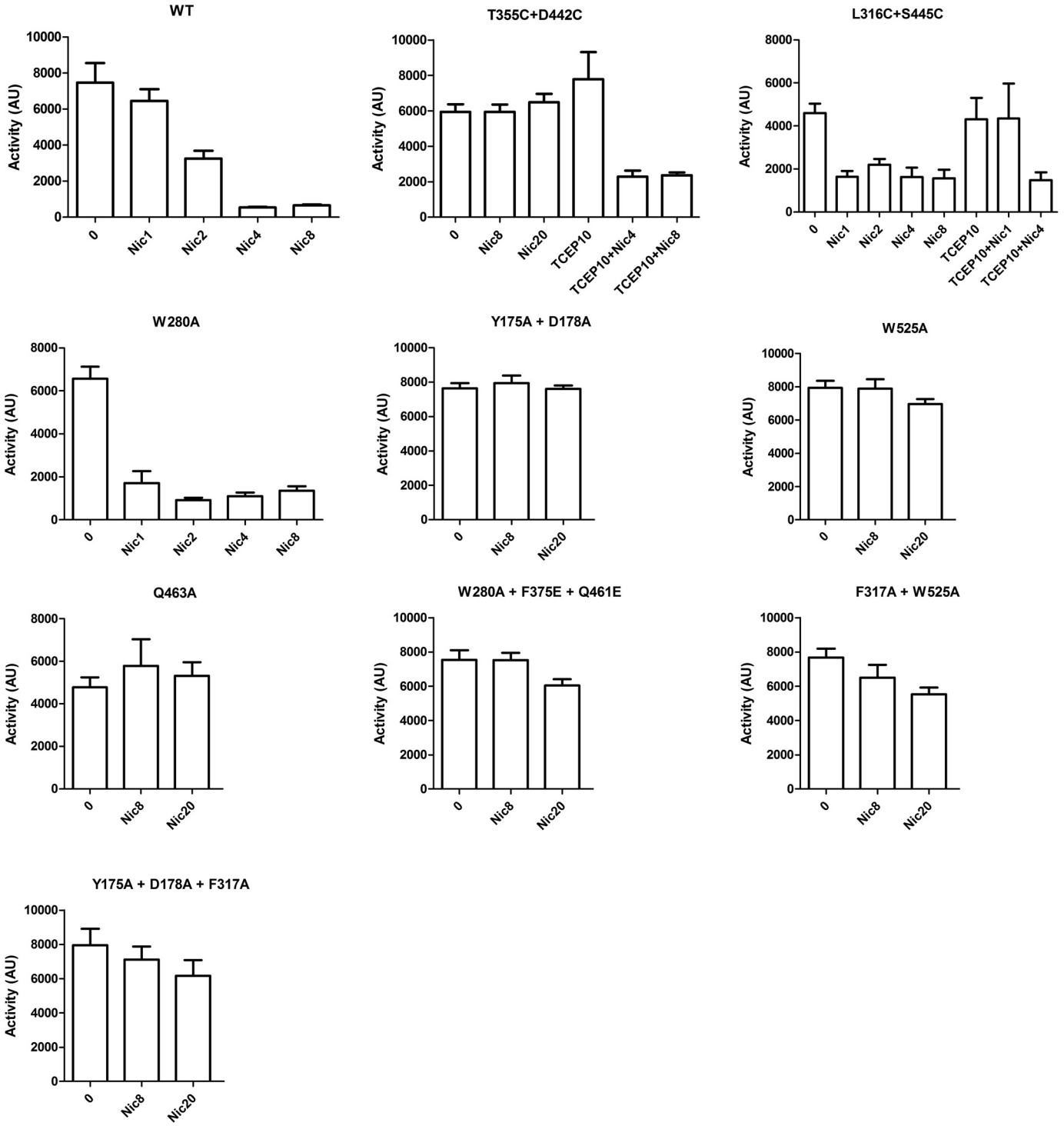

FIGURE 5. **β-galactosidase activities of the recombinant strains harboring BvgS variants with substitutions in the periplasmic domains.** The *ptx-lacZ* reporter was used to determine the basal activity and response to nicotinate. The data for the recombinant strains harboring $BvgS_{C355\text{-}C442}$ or $BvgS_{Q463A}$ are from Ref. 21. The concentrations of nicotinate in the growth medium are given in micromolar. The reducing agent tris(2-carboxyethyl)phosphine was added to the cultures at 10 mM when indicated. Note that tris(2-carboxyethyl)phosphine has no effect on WT BvgS (21). The measurements were performed at least three times, and the mean ± S.E. are shown. They are expressed in arbitrary enzymatic units, calculated as described in Ref. 22.

sitive to nicotinate, consistent with the inability of the modified VFT2 cavity to accommodate nicotinate (14) (Fig. 5). F317A in the VFT2cavity that causes a hypersensitive phenotype (14) was combined with W525A in VFT2, which causes an unresponsive phenotype. This yielded a BvgS variant insensitive to nicotinate (Fig. 5). We also combined the same F317A substitution in VFT2 with D175A/Y178A in $VFT1_{L2}$, which gives an unresponsive phenotype. The resulting variant is also not responsive to nicotinate. The similar phenotypes of the latter two variants show that enhanced nicotinate binding cannot compensate for the increased slackness of the second lobe of VFT1 or the first lobe of VFT2. Together, the data support the idea that nicotinate causes a con-

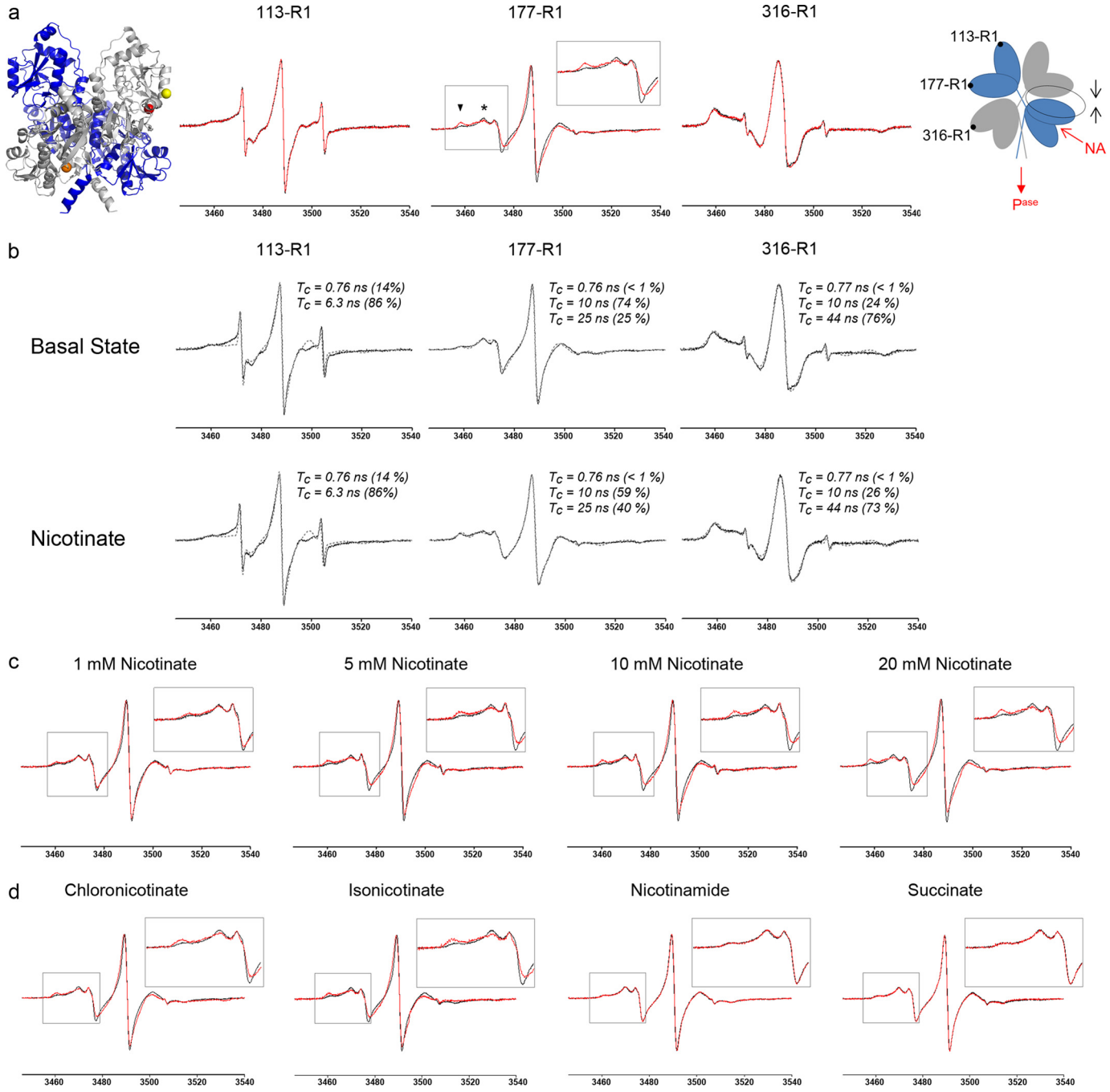

FIGURE 6. **Nicotinate affects the dynamics of the second VFT1 lobe *in vitro*, as shown by CWEPR.** *a*, *left panel*, the model indicates the positions of the spin labels, called R1, in BvgS-p. One monomer is shown in *blue* and the other in *gray*. The spheres (*yellow* for 113-R1, *red* for 177-R1, and *orange* for 316-R1) are centered on the C α of the respective residues in one monomer. *Center panel*, the normalized spectra of BvgS-p variants alone (*black*) or in the presence of 20 mM nicotinate (*red*) are shown, with the position of the spin probe indicated above. The magnetic field is in gauss. The *inset* presents an enlargement of the first part of the spectrum (*boxed region*). The *arrowheads* and *asterisks* indicate the slow and fast components, respectively. *Right panel*, the schematic represents the modification of Bvg-p after nicotinate (*NA*) perception. The increase of the slow component in the BvgS-$p_{177\text{-}R1}$ spectrum suggests the strengthening (*convergent arrows*) of the $VFT1_{L2}$-$VFT2_{L1}$ interface (*oval*). The resulting compact block formed by the VFT2s and the $VFT1_{L2s}$ affects the H19 helices so that the cytoplasmic moiety shifts to the phosphatase mode (P^{ase}). *b*, the spectra in *a* were simulated and are shown in *stippled gray lines* on top of the recorded spectra in *full black lines*. The correlation times (nanoseconds) of the spectral components and the occupancy of each state (percent) are indicated. *c*, spectra of BvgS-p_{177R1} with 1, 5, 10, or 20 mM nicotinate. The effect of nicotinate is detected at the same concentrations as *in vivo*. *d*, effects of various compounds on the spectrum of BvgS-p_{177R1}, all used at 20 mM. Chloronicotinate and isonicotinate are *in vivo* modulators, unlike nicotinamide and succinate.

formational transition involving most of the periplasmic domain, whose integrity is necessary to trigger the shift of the cytoplasmic moiety from kinase to phosphatase mode.

Interdomain Communication Probed by EPR Spectroscopy—To detect changes of the conformation and dynamics of the periplasmic domains caused by nicotinate binding, we performed site-directed spin labeling and CWEPR experiments. We used single Cys BvgS-p variants that retain WT BvgS activity and response to modulation (21) and covalently labeled them with the sulfhydryl-reactive spin probe MTSL (Fig. 6). The modified Cys residue is called R1. BvgS-p does not contain natural Cys residues, and, therefore, the labeling is site-specific.

The four Cys side chains are surface-exposed and located on the outer rims of the lobes. Three of them (113 in $VFT1_{L1}$, 177 in $VFT1_{L2}$, and 316 in $VFT2_{L1}$) were labeled successfully (Fig. 6*a*), whereas hardly any labeling of Cys^{442} in $VFT2_{L2}$ was obtained. The shapes of CWEPR spectra at room temperature provide information on the conformation and the overall mobility of the spin label, which depends on its position on the protein (33). Because the VFT lobes form rigid bodies, the CWEPR spectra will reflect the rates at which the spin label experiences changes in its environment, which depends on its own motions and on the dynamic properties of the region to which it is attached (34, 35).

The spectrum of BvgS-$p_{113\text{-}R1}$ (*i.e.* with a spin label at position 113 in $VFT1_{L1}$) is composed of sharp peaks, indicating rather fast nitroxide motions (Fig. 6*a*). Accordingly, the rotational correlation times of the spin label are in the nanosecond range (Fig. 6*b*). For BvgS-$p_{177\text{-}R1}$ with a spin label in $VFT1_{L2}$, the spectrum is broader, and the peaks are less sharp, showing that the second lobe of VFT1 has a more limited mobility (Fig. 6*a*). Finally, for BvgSp-$_{316\text{-}R1}$ with a spin label in $VFT2_{L1}$, the CWEPR spectrum mainly shows a broad peak, indicating a conformational ensemble of very limited dynamics (Fig. 6*a*). The high rotational correlation time of the major form indicates that the reorientational motions of the nitroxide are completely restricted (Fig. 6*b*). In all three cases, the occurrence of several spectral components may reflect conformational heterogeneity.

The addition of nicotinate modestly but reproducibly increases the proportion of the slow-mobility spectral component and decreases that of the fast one for BvgS-$p_{177\text{-}R1}$ (Fig. 6*a*). This effect is seen at concentrations similar to those that modulate BvgS *in vivo* (Fig. 6*c*). The low amplitude of the changes may be due to the weak affinity of the BvgS-nicotinate interaction, but the high reproducibility of the results makes such changes meaningful. To validate our observation, we used other modulators, chloronicotinate and isonicotinate, and two non-modulating molecules, nicotinamide and succinate (11). The latter two cause no detectable spectral changes, whereas the former have the same effect as nicotinate (Fig. 6*d*). The fact that the binding of modulators to VFT2 decreases the mobility of the second lobes of the VFT1s demonstrates long-distance, mechanical communication between domains. The observation that the very restrained mobility of the VFT2s negatively affects the dynamics of the $VFT1_{L2s}$ also suggests that the $VFT1_{L2}$-VFT2 interfaces tighten in the modulated state. This is in line with earlier findings indicating that the integrity of the VFT1-VFT2 interfaces is necessary for the response to modulation (21). For the other two positions of the spin probe, the addition of nicotinate does not affect the spectra (Fig. 6*a*). Therefore, the mobility of the spin label in $VFT1_{L1}$ remains fast in the presence of the modulator, as seen with BvgS-$p_{113\text{-}R1}$. As for BvgS-$p_{316\text{-}R1}$, the spectrum does not change, most likely because the mobility regime of R1 at position 316 is already near the rigid limit in the basal state (Fig. 6*b*).

We used EPR to analyze the effects of specific substitutions that make BvgS insensitive to nicotinate. Therefore, we first tested the F375E+Q461E substitutions in VFT2 that hamper nicotinate binding. The spectra of the BvgS-$p_{F375E+Q461E}$ variants with R1 at positions 177 or 316 are similar to those of their WT counterparts (Fig. 7*a*). Unlike with the WT protein, nicotinate does not modify the spectrum of BvgS-$p_{177\text{-}R1}$ with the spin probe in $VFT1_{L2}$ (Fig. 7*b*). We then selected substitutions that affect signaling rather than nicotinate binding. The side chain of Gln^{463} in $VFT2_{L2}$ interacts with $VFT1_{L2}$ of the other monomer and with the hinge within VFT2 (21). Its replacement with Ala increases the proportion of the fast spectral component of BvgS-p with a spin label at position 316 in $VFT2_{L1}$ (Fig. 7*a*). In addition, the broadening of the slow spectral component and the decrease of its rotational correlation time indicate a somewhat less constrained conformational ensemble (Fig. 7*c*). The CWEPR spectrum of BvgS-p with R1 at position 177 in $VFT1_{L2}$ is not modified by the Q463A substitution. Unlike that of the WT protein, however, it is not affected by nicotinate (Fig. 7*b*). This substitution therefore appears to make VFT2 a little more slack and to disrupt interactions that participate in inter-VFT2-VFT1 communication.

The W525A substitution in $VFT2_{L1}$ increases the proportion of the slow component of the BvgS-p spectrum with the spin label at position 177 (Fig. 7, *a* and *c*). In contrast, the spectrum of BvgS-p with the label at position 316 in $VFT2_{L1}$ is not modified by the W525A substitution. Neither is affected by the addition of nicotinate (Fig. 7*b*). The somewhat reduced dynamics of the spin probe in $VFT1_{L2s}$ suggests that disrupting the structural integrity of the $VFT2_{L1s}$ by the W525A substitution enhances $VFT1_{L2}$-$VFT2_{L1}$ contacts. *In vivo*, however, BvgS does not react to the presence of nicotinate, probably because the VFT2s are more slack. We also tested the substitutions D175A/Y178A in $VFT1_{L2}$, which revealed an increased proportion of the high-mobility component in the spectrum of BvgS-p with a label at position 316 in $VFT2_{L1}$ and a slight decrease of the slow mobility one (Fig. 7, *a* and *c*). Nicotinate does not modify the spectrum (Fig. 7*b*). Therefore, the slacker $VFT1_{L2s}$ slightly increase the $VFT2_{L1s}$ dynamics, which might cause the unresponsive phenotype of this variant. These substitutions were not tested in BvgS-$p_{177\text{-}R1}$ because their proximity to the spin probe was liable to cause local effects. CWEPR shows specific alterations of the conformation and dynamics of the VFT domains, which are related to the phenotypes of the nicotinate-unresponsive variants.

Discussion

BvgS regulates the pathogenicity of *B. pertussis*. In response to specific cues, BvgS shifts from a kinase mode of activity, in which expression of the virulence genes is maximal, to a phosphatase mode, in which the bacteria are avirulent. We have shown previously that the default kinase activity of BvgS depends on its periplasmic moiety exerting a strain onto the transmembrane α helices (21). The strain maintains those helices in specific conformation and dynamics that consequently determine the mode of activity of the cytoplasmic enzymatic moiety. Here we characterized the changes of the BvgS VFTs in response to the modulator nicotinate and identified structural features of the periplasmic domain involved in the transition.

The natural ligands of BvgS and the *in vivo* niches or conditions in which its activity is regulated remain unknown. However, the ability of BvgS to shift from kinase to phosphatase is conserved among *B. pertussis* clinical isolates (13), arguing that

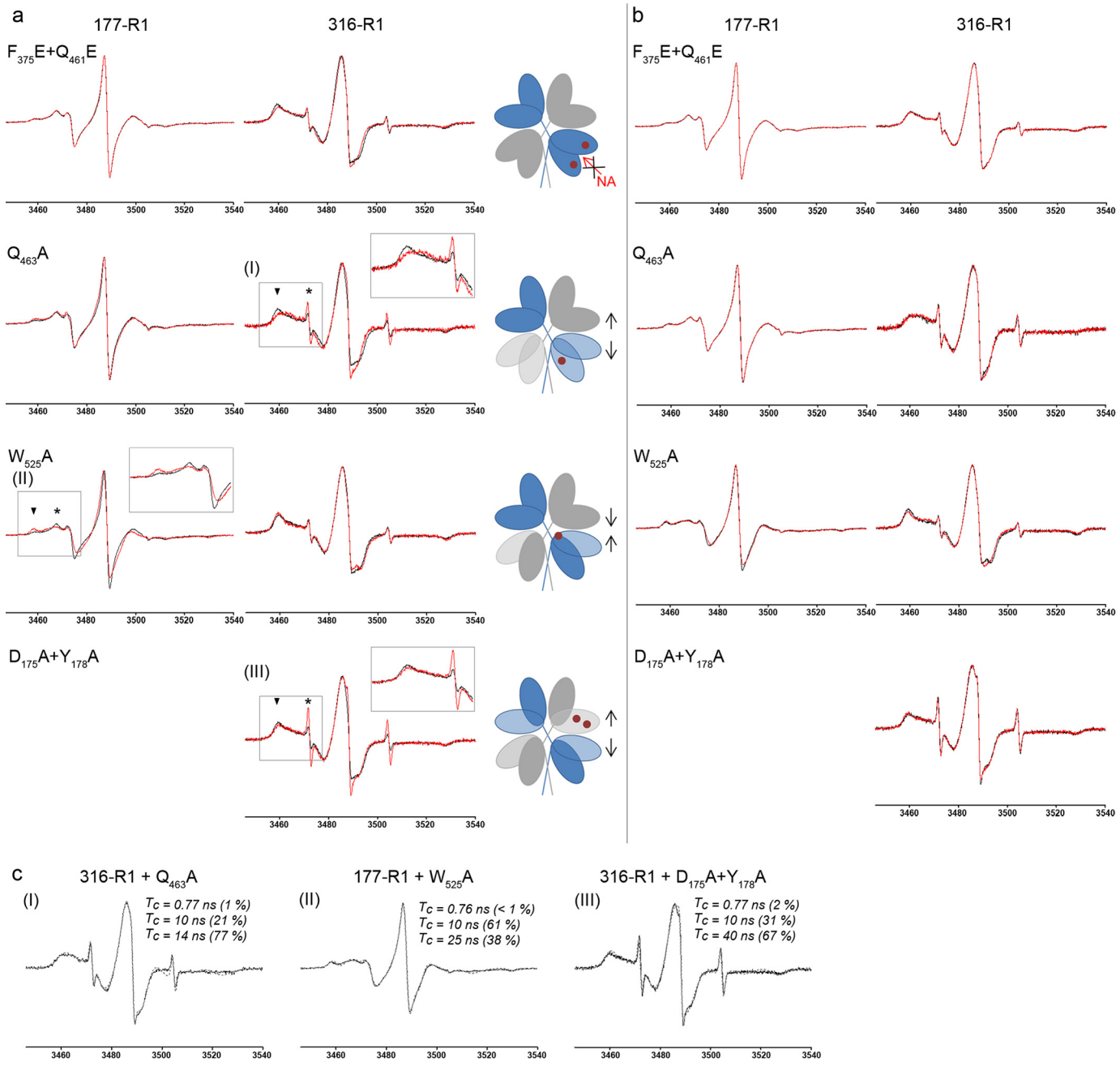

FIGURE 7. **Specific substitutions that make BvgS unresponsive to nicotinate affect BvgS-p dynamics *in vitro*.** *a*, the CWEPR spectra (*black*) of WT BvgS-$p_{177\text{-}R1}$ or BvgS-$p_{316\text{-}R1}$ are superimposed onto those (*red*) of the indicated variants labeled at the same positions. See Fig. 6 for details. The schematics on the *right* show the positions of the substitutions (*brown dots*) and provide interpretations of their effects (shown only for one side of the dimer). Lobes colored in paler shades of *blue* or *gray* are slackened by the substitutions relative to the WT protein. *First row*, the F375E/Q461E substitutions at the surface of the cavity hinder nicotinate binding (*crossed arrow* between nicotinate (*NA*) and BvgS). *Second row*, the Q463A substitution slackens the VFT2s. The looser VFT2-$VFT1_{L2}$ interface that presumably results from slacker VFT2s is represented by *divergent arrows*. *Third row*, the small mobility decrease of $VFT1_{L2}$ is most likely caused by the W525A substitution loosening the $VFT2_{L1}$ away from the center of the dimer, therefore enabling its closer contacts with $VFT1_{L2}$ (*convergent arrows*). *Fourth row*, the D175A/Y178A substitutions in $VFT1_{L2}$ slightly increase the mobility of $VFT2_{L1}$, likely because of looser interlobe contacts (*divergent arrows*). *b*, the effect of nicotinate on the CWEPR spectra of the BvgS-p alone (*black*) or in the presence of 20 mM nicotinate (*red*). *Second row*, the Q463A substitution slackens the VFT2s (see *a*), and, consequently, nicotinate addition does not affect the BvgS-$p_{177\text{-}R1}$ spectrum, unlike for the WT protein. *Third row*, similarly, the slackened $VFT2s_{W525A}$ prevents the effect of nicotinate on BvgS-$p_{177\text{-}RI}$. *Fourth row*, the D175A/Y178A substitutions in $VFT1_{L2}$ make the VFT2s slacker (see *a*), and nicotinate does not rigidify them. *c*, spectra of interest were simulated as described in Fig. 6.

the bacterium down-modulates virulence factors expression at some point during its infectious cycle. Moreover, the residues that line the VFT cavities are invariant (13), strongly arguing that they perceive ligands *in vivo*, in line with the classical binding paradigm of VFT domains (16). In the absence of *bona fide* ligands, nicotinate has served here as a model signal to decipher the molecular mechanisms of sensory transduction. We hypothesize that the mechanistic principles revealed by this study will also be true for the natural BvgS ligands.

The conformations and dynamics of the periplasmic domain of BvgS differ between the basal and the nicotinate-bound states. EPR shows that nicotinate binding to the VFT2s induces

long-distance changes in the periplasmic domain of BvgS, notably by decreasing the mobility of the second VFT1 lobes. Their reduced dynamics probably stem from the formation of tighter VFT2-$VFT1_{L2}$ interfaces, with the rigid VFT2s affecting the conformation and dynamics of the $VFT1_{L2s}$. The resulting rigid VFT2-$VFT1_{L2}$ block most likely impacts the H19 helices, causing a shift of the cytoplasmic moiety of BvgS to the phosphatase mode. The loss of kinase activity upon closing the VFT1 cavities suggests that the VFT1s might be the true environmental sensors of BvgS (21). If this is the case, we hypothesize that ligand binding to VFT1 affects the conformation and dynamics of the periplasmic moiety in a similar manner, with the same consequences for the enzymatic moiety as for those caused by nicotinate.

We identified two groups of BvgS variants with a modified response to nicotinate. There are a few hypersensitive variants. They include $BvgS_{F317A}$ (14), $BvgS_{C316\text{-}C445}$ with an S-S bond across VFT2 (this work), and $BvgS_{W280A}$ (this work). The first substitution enhances the binding of nicotinate to the VFT2 cavity (14). For the second variant, it is likely that the conformational change of VFT2 upon nicotinate binding is facilitated by the S-S bond-induced constraint. Finally, $BvgS_{W280A}$ indicates that looser $VFT1_{L1s}$ promotes the changes of the periplasmic moiety caused by nicotinate. We also generated a larger number of insensitive variants. Substitutions that abolish the *in vivo* response to nicotinate have specific *in vitro* effects on BvgS-p, as seen by CWEPR. Such substitutions slacken the VFT lobes or weaken the connections between domains. This argues that the shift to phosphatase in response to nicotinate implies a tense structural transition involving a large part of the periplasmic moiety of BvgS. Nicotinate cannot exert its effect on the insensitive variants, most likely because the VFT2-$VFT1_{L2}$ block is slackened by the substitutions.

In addition to the Bvg^- and Bvg^+ phases, *B. pertussis* can be in an intermediate phase, in which a subset of virulence factors are expressed together with specific intermediate genes (5, 7–9). *In vitro*, intermediate levels of activity occur at intermediate concentrations of nicotinate. Nevertheless, we propose that BvgS exists in two distinct, stable states that interconvert rather than in several different states. According to the two-state model, the kinase state of BvgS is overwhelmingly populated in the Bvg^+ phase, the phosphatase state is overwhelmingly populated in the Bvg^- phase, and intermediate levels of activity correspond to the two states being populated simultaneously. In the default kinase state of BvgS, the periplasmic moiety exerts a strain on the transmembrane helices. Substitutions such as W535A or R472A/Y473A that weaken the connections between $VFT2_{L2s}$ and the transmembrane helices cause BvgS to shift to the phosphatase mode without a modulator (21). We propose that, similarly, nicotinate binding disrupts periplasmic interactions essential to maintain the cytoplasmic moiety in the kinase mode. This disruption allows the transmembrane helices to rearrange in a stable manner, and their modified conformation and dynamics therefore set the cytoplasmic moiety to the phosphatase mode. The possibility that the intermediate states of activity of BvgS correspond to as many distinct conformational states of the transmembrane helices and of the cytoplasmic moiety cannot be ruled out but would be complicated.

The nature of the changes that take place in the cytoplasmic moiety of BvgS upon transitions between the kinase and phosphatase states remains to be determined. Recent studies on model two-component sensor kinases have indicated that signaling implies reciprocal displacements of the helical linkers that precede the kinase domain and that the dimerization/histidine phosphotransfer DHp helices undergo dynamic conformational changes between the kinase and phosphatase states (36–39). In BvgS, the PAS domain between the transmembrane region and the DHp domain of the kinase must relay the information from the periplasmic moiety to the enzymatic moiety. The BvgS PAS dimerizes (26). The dimeric PAS domains of other sensor proteins have been shown to undergo quaternary structure changes upon signaling (40–44). The segment between the PAS and the kinase domains is predicted to form a two-helix coiled coil that extends into the DHp domain, and a specific substitution that disrupts the connection between the PAS domains and those α helices abrogates kinase activity (26). This suggests that the relaxed, *i.e.* the most stable, interface of the coiled coil preceding the enzymatic moiety corresponds to the phosphatase mode. In the kinase mode, the specific quaternary arrangement of the PAS domains dictated by the transmembrane helices most likely antagonizes the relaxed conformation of that coiled coil. We therefore propose that nicotinate binding to the periplasmic domain triggers a rearrangement of the PAS domain interface in such a manner that the coil between the PAS and the kinase can adopt its most stable conformation, corresponding to the phosphatase mode.

BvgS is the prototype of a large family of VFT-containing sensor kinases. There are hundreds of BvgS homologs with tandem VFT domains, and, therefore, the mechanistic principles identified in this work are likely to be relevant for them as well. Among other signaling proteins with extracellular VFT domains in tandem are notably the ionotropic Glu receptors of higher eukaryotes. The regulation of ionotropic Glu receptor channel activity by the binding of ligands has been studied extensively (45–48), and it differs from the mechanisms found here for BvgS. Interestingly, the x-ray structure of the periplasmic portion of BvgS shows a tighter arrangement of its VFT domains than in ionotropic Glu receptors (21). This work confirms that a compact extracytoplasmic moiety with tight interactions between VFT domains is essential for signaling by BvgS-like proteins.

Author Contributions—E. D. and E. L. designed and performed the experiments and analyzed the data shown in Figs. 2 and 5. E. L., E. D., J. G., and H. V. designed and performed the experiments and analyzed the data shown in Figs. 6 and 7. A. V. and E. D. designed and performed the experiments and analyzed the data shown in Fig. 3. M. F. L., G. B., and J. d. R. designed and performed the experiments and analyzed the data shown in Fig. 4. F. J. D., R. A., C. L., and E. D. conceived the study. F. J. D. coordinated the study and wrote the paper. All authors reviewed and approved the manuscript.

Acknowledgments—We thank J. Herrou for preliminary mutagenesis data and the "Plateforme d'Interactions Moléculaires de l'Université de Lille 2" for MST measurements and analyses.

References

1. Stock, A. M., Robinson, V. L., and Goudreau, P. N. (2000) Two-component signal transduction. *Annu. Rev. Biochem.* **69,** 183–215
2. Capra, E. J., and Laub, M. T. (2012) Evolution of two-component signal transduction systems. *Annu. Rev. Microbiol.* **66,** 325–347
3. Gao, R., and Stock, A. M. (2009) Biological insights from structures of two-component proteins. *Annu. Rev. Microbiol.* **63,** 133–154
4. Krell, T., Lacal, J., Busch, A., Silva-Jiménez, H., Guazzaroni, M. E., and Ramos, J. L. (2010) Bacterial sensor-kinases: diversity in the recognition of environmental signals. *Annu. Rev. Microbiol.* **64,** 539–559
5. Cotter, P. A., and Jones, A. M. (2003) Phosphorelay control of virulence gene expression in *Bordetella*. *Trends Microbiol.* **11,** 367–373
6. Melvin, J. A., Scheller, E. V., Miller, J. F., and Cotter, P. A. (2014) *Bordetella pertussis* pathogenesis: current and future challenges. *Nat. Rev. Microbiol.* **12,** 274–288
7. Cotter, P. A., and Miller, J. F. (1997) A mutation in the *Bordetella bronchiseptica bvgS* gene results in reduced virulence and increased resistance to starvation, and identifies a new class of Bvg-regulated antigens. *Mol. Microbiol.* **24,** 671–685
8. Stockbauer, K. E., Fuchslocher, B., Miller, J. F., and Cotter, P. A. (2001) Identification and characterization of BipA, a *Bordetella* Bvg-intermediate phase protein. *Mol. Microbiol.* **39,** 65–78
9. Jones, A. M., Boucher, P. E., Williams, C. L., Stibitz, S., and Cotter, P. A. (2005) Role of BvgA phosphorylation and DNA binding affinity in control of Bvg-mediated phenotypic phase transition in *Bordetella pertussis*. *Mol. Microbiol.* **58,** 700–713
10. Schneider, D. R., and Parker, C. D. (1982) Effect of pyridines on phenotypic properties of *Bordetella pertussis*. *Infect. Immun.* **38,** 548–553
11. Melton, A. R., and Weiss, A. A. (1993) Characterization of environmental regulators of *Bordetella pertussis*. *Infect. Immun.* **61,** 807–815
12. Martínez de Tejada, G. M., Miller, J. F., and Cotter, P. A. (1996) Comparative analysis of the virulence control systems of *Bordetella pertussis* and *Bordetella bronchiseptica*. *Mol. Microbiol.* **22,** 895–908
13. Herrou, J., Debrie, A. S., Willery, E., Renaud-Mongénie, G., Locht, C., Mooi, F., Jacob-Dubuisson, F., and Antoine, R. (2009) Molecular evolution of the two-component system BvgAS involved in virulence regulation in *Bordetella*. *PLoS ONE* **4,** e6996
14. Herrou, J., Bompard, C., Wintjens, R., Dupré, E., Willery, E., Villeret, V., Locht, C., Antoine, R., and Jacob-Dubuisson, F. (2010) Periplasmic domain of the sensor-kinase BvgS reveals a new paradigm for the Venus flytrap mechanism. *Proc. Natl. Acad. Sci. U.S.A.* **107,** 17351–17355
15. Jacob-Dubuisson, F., Wintjens, R., Herrou, J., Dupré, E., and Antoine, R. (2012) in *Two-component System in Bacteria* (Gross, R., and Beier, D., eds) pp 57–83, Caister Academic Press, Norfolk, UK
16. Quiocho, F. A., and Ledvina, P. S. (1996) Atomic structure and specificity of bacterial periplasmic receptors for active transport and chemotaxis: variation of common themes. *Mol. Microbiol.* **20,** 17–25
17. Kristensen, A. S., Geballe, M. T., Snyder, J. P., and Traynelis, S. F. (2006) Glutamate receptors: variation in structure-function coupling. *Trends Pharmacol. Sci.* **27,** 65–69
18. Ahier, A., Rondard, P., Gouignard, N., Khayath, N., Huang, S., Trolet, J., Donoghue, D. J., Gauthier, M., Pin, J. P., and Dissous, C. (2009) A new family of receptor tyrosine kinases with a Venus flytrap binding domain in insects and other invertebrates activated by aminoacids. *PLoS ONE* **4,** e5651
19. Trakhanov, S., Vyas, N. K., Luecke, H., Kristensen, D. M., Ma, J., and Quiocho, F. A. (2005) Ligand-free and -bound structures of the binding protein (LivJ) of the *Escherichia coli* ABC leucine/isoleucine/valine transport system: trajectory and dynamics of the interdomain rotation and ligand specificity. *Biochemistry* **44,** 6597–6608
20. Neiditch, M. B., Federle, M. J., Pompeani, A. J., Kelly, R. C., Swem, D. L., Jeffrey, P. D., Bassler, B. L., and Hughson, F. M. (2006) Ligand-induced asymmetry in histidine sensor kinase complex regulates quorum sensing. *Cell* **126,** 1095–1108
21. Dupré, E., Herrou, J., Lensink, M. F., Wintjens, R., Vagin, A., Lebedev, A., Crosson, S., Villeret, V., Locht, C., Antoine, R., and Jacob-Dubuisson, F. (2015) Virulence regulation with Venus Flytrap domains: structure and function of the periplasmic moiety of the sensor-kinase BvgS. *PLoS Pathog.* **11,** e1004700
22. Antoine, R., Alonso, S., Raze, D., Coutte, L., Lesjean, S., Willery, E., Locht, C., and Jacob-Dubuisson, F. (2000) New virulence-activated and virulence-repressed genes identified by systematic gene inactivation and generation of transcriptional fusions in *Bordetella pertussis*. *J. Bacteriol.* **182,** 5902–5905
23. Karimova, G., Pidoux, J., Ullmann, A., and Ladant, D. (1998) A bacterial two-hybrid system based on a reconstituted signal transduction pathway. *Proc. Natl. Acad. Sci. U.S.A.* **95,** 5752–5756
24. Huth, J. R., Bewley, C. A., Jackson, B. M., Hinnebusch, A. G., Clore, G. M., and Gronenborn, A. M. (1997) Design of an expression system for detecting folded protein domains and mapping macromolecular interactions by NMR. *Protein Sci.* **6,** 2359–2364
25. Turnbull, W. B., and Daranas, A. H. (2003) On the value of c: can low affinity systems be studied by isothermal titration calorimetry? *J. Am. Chem. Soc.* **125,** 14859–14866
26. Dupré, E., Wohlkonig, A., Herrou, J., Locht, C., Jacob-Dubuisson, F., and Antoine, R. (2013) Characterization of the PAS domain in the sensor-kinase BvgS: mechanical role in signal transmission. *BMC Microbiol.* **13,** 172
27. Stoll, S., and Schweiger, A. (2006) EasySpin, a comprehensive software package for spectral simulation and analysis in EPR. *J. Magn. Reson.* **178,** 42–55
28. Jones, G., Willett, P., and Glen, R. C. (1995) Molecular recognition of receptor sites using a genetic algorithm with a description of desolvation. *J. Mol. Biol.* **245,** 43–53
29. Hess, B., Kutzner, C., van der Spoel, D., and E., L. (2008) GROMACS 4: algorithms for highly efficient, load-balanced, and scalable molecular simulation. *J. Chem. Theory Comput.* **4,** 435–447
30. Boulanger, A., Chen, Q., Hinton, D. M., and Stibitz, S. (2013) *In vivo* phosphorylation dynamics of the *Bordetella pertussis* virulence-controlling response regulator BvgA. *Mol. Microbiol.* **88,** 156–172
31. Jerabek-Willemsen, M., Wienken, C. J., Braun, D., Baaske, P., and Duhr, S. (2011) Molecular interaction studies using microscale thermophoresis. *Assay Drug Dev. Technol.* **9,** 342–353
32. Seidel, S. A., Dijkman, P. M., Lea, W. A., van den Bogaart, G., Jerabek-Willemsen, M., Lazic, A., Joseph, J. S., Srinivasan, P., Baaske, P., Simeonov, A., Katritch, I., Melo, F. A., Ladbury, J. E., Schreiber, G., Watts, A., Braun, D., and Duhr, S. (2013) Microscale thermophoresis quantifies biomolecular interactions under previously challenging conditions. *Methods* **59,** 301–315
33. Mchaourab, H. S., Lietzow, M. A., Hideg, K., and Hubbell, W. L. (1996) Motion of spin-labeled side chains in T4 lysozyme: correlation with protein structure and dynamics. *Biochemistry* **35,** 7692–7704
34. Hubbell, W. L., Cafiso, D. S., and Altenbach, C. (2000) Identifying conformational changes with site-directed spin labeling. *Nat. Struct. Biol.* **7,** 735–739
35. Rice, A. J., Alvarez, F. J., Schultz, K. M., Klug, C. S., Davidson, A. L., and Pinkett, H. W. (2013) EPR spectroscopy of MolB2C2-a reveals mechanism of transport for a bacterial type II molybdate importer. *J. Biol. Chem.* **288,** 21228–21235
36. Molnar, K. S., Bonomi, M., Pellarin, R., Clinthorne, G. D., Gonzalez, G., Goldberg, S. D., Goulian, M., Sali, A., and DeGrado, W. F. (2014) Cys-scanning disulfide crosslinking and Bayesian modeling probe the transmembrane signaling mechanism of the histidine kinase, PhoQ. *Structure* **22,** 1239–1251
37. Wang, C., Sang, J., Wang, J., Su, M., Downey, J. S., Wu, Q., Wang, S., Cai, Y., Xu, X., Wu, J., Senadheera, D. B., Cvitkovitch, D. G., Chen, L., Goodman, S. D., and Han, A. (2013) Mechanistic insights revealed by the crystal structure of a histidine kinase with signal transducer and sensor domains. *PLoS Biol.* **11,** e1001493
38. Ferris, H. U., Coles, M., Lupas, A. N., and Hartmann, M. D. (2014) Crystallographic snapshot of the *Escherichia coli* EnvZ histidine kinase in an active conformation. *J. Struct. Biol.* **186,** 376–379
39. Mechaly, A. E., Sassoon, N., Betton, J. M., and Alzari, P. M. (2014) Segmental helical motions and dynamical asymmetry modulate histidine kinase autophosphorylation. *PLoS Biol.* **12,** e1001776

40. King, H. A., Hoelz, A., Crane, B. R., and Young, M. W. (2011) Structure of an enclosed dimer formed by the *Drosophila* period protein. *J. Mol. Biol.* **413,** 561–572
41. Little, R., Salinas, P., Slavny, P., Clarke, T. A., and Dixon, R. (2011) Substitutions in the redox-sensing PAS domain of the NifL regulatory protein define an inter-subunit pathway for redox signal transmission. *Mol. Microbiol.* **82,** 222–235
42. Slavny, P., Little, R., Salinas, P., Clarke, T. A., and Dixon, R. (2010) Quaternary structure changes in a second Per-Arnt-Sim domain mediate intramolecular redox signal relay in the NifL regulatory protein. *Mol. Microbiol.* **75,** 61–75
43. Möglich, A., Ayers, R. A., and Moffat, K. (2009) Structure and signaling mechanism of Per-ARNT-Sim domains. *Structure* **17,** 1282–1294
44. Ayers, R. A., and Moffat, K. (2008) Changes in quaternary structure in the signaling mechanisms of PAS domains. *Biochemistry* **47,** 12078–12086
45. Karakas, E., and Furukawa, H. (2014) Crystal structure of a heterotetrameric NMDA receptor ion channel. *Science* **344,** 992–997
46. Lee, C. H., Lü, W., Michel, J. C., Goehring, A., Du, J., Song, X., and Gouaux, E. (2014) NMDA receptor structures reveal subunit arrangement and pore architecture. *Nature* **511,** 191–197
47. Meyerson, J. R., Kumar, J., Chittori, S., Rao, P., Pierson, J., Bartesaghi, A., Mayer, M. L., and Subramaniam, S. (2014) Structural mechanism of glutamate receptor activation and desensitization. *Nature* **514,** 328–334
48. Yelshanskaya, M. V., Li, M., and Sobolevsky, A. I. (2014) Structure of an agonist-bound ionotropic glutamate receptor. *Science* **345,** 1070–1074